

## Article

# Examination of Using Aluminum-Foam/Finned-Tube Beds Packed with Maxsorb III for Adsorption Ice Production System

Mahmoud Badawy Elsheniti <sup>1,2,\*</sup>, Mohamed Shaaban Eissa <sup>2</sup>, Hany Al-Ansary <sup>1,3</sup>, Jamel Orfi <sup>1,3</sup>, Osama Elsamni <sup>2</sup> and Abdelrahman El-Leathy <sup>1,4</sup>

- <sup>1</sup> Mechanical Engineering Department, College of Engineering, King Saud University, Riyadh 11451, Saudi Arabia; hansary@ksu.edu.sa (H.A.-A.); orfij@ksu.edu.sa (J.O.); aelleathy@ksu.edu.sa (A.E.-L.)
- <sup>2</sup> Mechanical Engineering Department, Faculty of Engineering, Alexandria University, Alexandria 21544, Egypt; eng.mohamed.shabaan@alexu.edu.eg (M.S.E.); elsamni@alexu.edu.eg (O.E.)
- <sup>3</sup> K.A.CARE Energy Research and Innovation Center, King Saud University, Riyadh 11451, Saudi Arabia
- <sup>4</sup> Mechanical Power Engineering Department, Faculty of Engineering, El-Matara, Helwan University, Cairo 11718, Egypt
- \* Correspondence: mbadawy.c@ksu.edu.sa

**Abstract:** Producing ice using adsorption systems can represent a sustainable solution and meet the recent global environmental regulations as they use natural refrigerants and can be driven by solar energy. However, the beds used in these systems still have low thermal and adsorption characteristics. This study investigates numerically the use of an emerging aluminum foamed bed packed with advanced Maxsorb adsorbent in a two-bed adsorption system and reports cases of performance improvements compared to the classical finned-tube based system used to produce ice. A comprehensive 2-D transient pressure distribution model for the two beds was developed and validated. The model considers the temporal and spatial variations of the two beds' parameters, while the effect of the thermal mass and heat transfer effectiveness of the condenser and evaporator components are imitated at the boundary conditions for bed openings using two zero-dimensional models. The results show the interrelated effects of varying the cycle times from 400 s to 1200 s with 2, 5, and 10 mm foam thicknesses/fin heights on the overall performance of both systems. The Al-foam based system demonstrated the performance superiority at a 2 mm foam thickness with maximum ice production of 49 kg<sub>ice</sub>/kg<sub>ads</sub> in 8 h, an increase of 26.6% over the counterpart finned-tube based system at a 400 s cycle time. The best COP of 0.366 was attained at a 5 mm foam thickness and 1200 s with an increase of 26.7%. The effective uptake of the Al-foam based system was reduced dramatically at a 10 mm foam thickness, which deteriorated the system performance.

**Keywords:** adsorption ice maker; metal foamed adsorber; finned tube; packed bed



**Citation:** Elsheniti, M.B.; Eissa, M.S.; Al-Ansary, H.; Orfi, J.; Elsamni, O.; El-Leathy, A. Examination of Using Aluminum-Foam/Finned-Tube Beds Packed with Maxsorb III for Adsorption Ice Production System. *Energies* **2022**, *15*, 2757. <https://doi.org/10.3390/en15082757>

Academic Editors: Wei-Hsin Chen, Aristotle T. Ubando, Chih-Che Chueh and Liwen Jin

Received: 28 February 2022

Accepted: 4 April 2022

Published: 8 April 2022

**Publisher's Note:** MDPI stays neutral with regard to jurisdictional claims in published maps and institutional affiliations.



**Copyright:** © 2022 by the authors. Licensee MDPI, Basel, Switzerland. This article is an open access article distributed under the terms and conditions of the Creative Commons Attribution (CC BY) license (<https://creativecommons.org/licenses/by/4.0/>).

## 1. Introduction

Ice production is essential for many applications in the refrigeration industry, including energy storage, food and vaccine preservation, and freeze desalination. In rural areas, transportation, fishing boats, and many other usages, there are needs for more efficient and thermally driven ice makers due to the limited electricity sources [1,2]. In addition, the current commonly used devices to produce ice are based on vapor compression cycles. These devices are highly electricity-consuming and use environmentally harmful refrigerants (HFCs, HCFCs) that contribute to aggravating global warming crises [3–5]. Adsorption refrigeration systems (ARSs) are considered environmentally friendly energy-saving systems that use low-quality thermal energy provided by solar or waste heat sources [6,7]. Furthermore, they can utilize natural refrigerants such as water and ethanol and require low maintenance efforts due to fewer moving parts. These ecological and practical merits

make them the most attractive and feasible way to meet the new international environmental regulations for refrigeration systems to a great extent [8,9]. However, ARSs in principle work under thermal swings between adsorption and regeneration processes. The thermal response along with adsorption kinetics in adsorption beds play a critical role in determining the cyclic transient operation performance of the ARS. Therefore, enhancing both thermal and adsorption characteristics of the adsorbent materials represents an active research area that aims at boosting the effective use of ARSs in different applications. Many investigations have been devoted to developing adsorbent beds with higher thermal performance including the use of a metal foam structure to accommodate the adsorbent material [10–12].

Metal-foam-based adsorbent beds have been proposed to enhance heat diffusion by conduction in the adsorbent domain via well-structured metal connectivity. This increases the effective thermal conductivity while providing high metal-to-adsorbent contact area and vapor permeability by foam cavities, and keeping good mechanical strength at higher foam thicknesses [13,14]. Mohammed et al. [15] experimentally tested aluminum foam packed with silica gel particles on a small scale for adsorption cooling applications and reported effective thermal conductivity of  $6 \text{ W}\cdot\text{m}^{-1}\cdot\text{K}^{-1}$  for the composite form. They developed a CFD model for the foam and silica gel domain and predicted a higher COP and SCP of 0.75 and  $827 \text{ W}\cdot\text{kg}^{-1}$ , respectively, due to the enhancement in the heat diffusion. Xu et al. [12] coated MIL-101 on copper foams and investigated experimentally the performance of a single tube and the effective thermal conductivity reached a maximum value of  $0.86 \text{ W}\cdot\text{m}^{-1}\cdot\text{K}^{-1}$ , causing a faster cooling rate of  $1.1 \text{ }^\circ\text{C}\cdot\text{s}^{-1}$ . Hu et al. [16] attained an effective thermal conductivity of  $2.89 \text{ W}\cdot\text{m}^{-1}\cdot\text{K}^{-1}$  by using aluminum foam packed with zeolite particles, which shortened the ARS cycle time. Pinheiro et al. [11] investigated numerically the performance of a single bed heat pump employing a copper foam coated bed with two advanced materials for heating applications: CPO-27(Ni) and SAPO-34, achieving  $27 \text{ W}\cdot\text{m}^{-1}\cdot\text{K}^{-1}$  effective thermal conductivity. The predicted SCP and COP were  $5130 \text{ W}\cdot\text{kg}^{-1}$  and 1.16 for CPO-27(Ni) and  $6877 \text{ W}\cdot\text{kg}^{-1}$  and 1.4 for SAPO-34, respectively. On the scale of system performance to produce ice, Jing et al. [17] used a lumped model to theoretically model a solar-powered refrigerator employing a charcoal/methanol pair and reached an evaporating temperature of  $-11.60 \text{ }^\circ\text{C}$ . Dakkama et al. [18] experimentally showed the potential of using CPO-27 (Ni)/water for ice making with production up to  $8.3 \text{ ton}\cdot\text{day}^{-1}\cdot\text{ton}_{\text{ads}}^{-1}$ . Qasem and El-Shaarawi [1] addressed the required factors to optimize the ice production from a solar adsorption system employing an activated-carbon/methanol pair and finned-tube adsorber under the climatic conditions of Dhahran. They concluded that using the right glazing cover, absorber tubes, and suitable tilt angle for the collector improved the solar COP from 0.12 to 0.24 and increased the ice production from 5 to  $13 \text{ kg}_{\text{ice}}\cdot\text{day}^{-1}$  per unit area of solar collectors. Hassan et al. [19] investigated using a thermodynamic model of the ice production from activated carbon/methanol ARS. The ice production ranged from  $0.6417\text{--}0.747 \text{ ton}\cdot\text{day}^{-1}\cdot\text{ton}_{\text{ads}}^{-1}$  at the regeneration temperature  $72\text{--}150 \text{ }^\circ\text{C}$ . Attalla et al. [20] investigated experimentally the activated carbon/methanol in a solar adsorption system for ice making and the system produced  $0.4 \text{ kg}_{\text{ice}}\cdot\text{kg}_{\text{ads}}^{-1}$ . Ji et al. [21] designed a solar ice-making adsorption system utilizing activated carbon/methanol and experimentally achieved  $8.4 \text{ kg}_{\text{ice}}\cdot\text{day}^{-1}$  at an  $-8.6 \text{ }^\circ\text{C}$  evaporating temperature.

Numerical simulations of the adsorbent beds are powerful tools that can be used to find out the effects of different geometrical parameters on ARS performance. In this regard, the thermodynamic and lumped models for ARSs cannot be used to study the effects of the adsorbent bed parameters such as fin spacing, bed height, and bed porosity. In addition, in such models, the spatial variations of temperature, pressure, and uptake are disregarded. Using lumped analytical models can extend the capability of lumped models to include parameters such as fin spacing and facilitate integration with other systems [22]. However, mass transfer resistances in the adsorbent bed are not included in these models. On the other hand, distributed-parameter CFD models include spatial variations of main variables

in the adsorbent bed and can be used as an effective tool to simulate the adsorbent bed performance [15]. Integrating such detailed bed models with zero-dimensional models for the evaporator and condenser components to mimic their pressure variations in a two-bed adsorption system can help in understanding the net effect of the geometrical and operating parameters, particularly when the evaporator pressure is a critical parameter [23].

The fin parameters have a considerable influence on heat and mass transfer through the adsorbent domain in the packed bed configuration. Rezk and Al-Dadah [22] studied the effect of fin spacing on the performance of a two-bed silica gel-water chiller in an empirical lumped analytical model. They found that reducing the fin spacing increased the cooling capacity by 3% and decreased the COP by 2.3%. A detailed numerical investigation was introduced by Elsheniti et al. [23] on a two-bed ARS using different fin numbers. They revealed that a specified fin number can be used to maximize the system COP. Nevertheless, reducing the fin spacing always led to increasing the specific cooling power. On the other hand, the metal foam thickness can affect the performance of ARS considerably. The COP was enhanced noticeably with increasing the foam thickness in a copper-foamed bed coated with two different materials, according to the numerical investigation conducted by Shaaban et al. [24].

Based on the current literature, the adsorbent materials and bed configurations are key elements for the ice production process. Activated carbon is the most common material used for adsorption of ice makers with different adsorbates. Maxsorb III type, known also as MSC-30 [25–27], is an advanced activated carbon type developed by the Kansai Coke and Chemicals Co. Ltd., Osaka, Japan. Maxsorb III consists of 95.13% C, 0.14% H, 0.25% N, 4.35% O and 0.13% Ash [28] and can be used with many refrigerants (methanol, R143a, ammonia and ethanol) [20]. It is a highly porous material of  $3200 \text{ m}^2 \cdot \text{g}^{-1}$  surface area and can reach an adsorption uptake of  $1.2 \text{ kg} \cdot \text{kg}^{-1}$  with ethanol,  $2 \text{ kg} \cdot \text{kg}^{-1}$  with HFC-134 [29], and  $1.3 \text{ kg} \cdot \text{kg}^{-1}$  with HFC-152A [30] and R507A [31], in addition to its fast kinetics [30,32]. However, Maxsorb III is characterized by low thermal conductivity and low packing density, which in turn can be considered as major limitations and affect adversely its performance at the system level [33,34]. Therefore, it is promising to increase the effective thermal conductivity of the Maxsorb III adsorbent bed, which has superior adsorption capacities, using the metal foam structure and investigate the net effect of such composite beds with enhanced mass and heat transfer characteristics on the overall performance of ARS for ice production.

In previous studies, the use of metal foamed beds showed a considerable enhancement in the ARS performance for normal cooling and heating applications, while it has not been investigated for adsorption ice production systems to the best of the authors' knowledge. To produce ice using an adsorption system, the adsorbent bed works under a lower pressure during the adsorption process compared to cooling and heating applications. The effect of adsorption pair isotherms and mass transfer mechanisms within the adsorbent bed on the system performance need to be examined at these low-pressure levels. Therefore, the present study introduces for the first time comparative computational investigations on using an aluminum foam bed (hereafter referred to as Al-foamed bed) packed with Maxsorb III in a granular form to produce ice. A 2-D transient distributed-parameter CFD model is developed using COMSOL Multiphysics to simulate the two adsorption beds simultaneously, while the time variation of the condenser and evaporator pressures are considered at the valve openings using zero-dimensional models for the two components. The new approach using the Al-foamed beds is compared with the classical finned adsorption beds used in the same adsorption ice production system. This investigation will help in understanding the interrelated effects of using metal foamed beds packed with Maxsorb III and the critical parametric options for the overall performance of an adsorption ice production system.

## 2. System Description

This study adopts a two-bed adsorption refrigeration system using an activated-carbon/ethanol pair to cool down ethylene glycol below  $-2\text{ }^{\circ}\text{C}$ . A schematic diagram of the system layout is illustrated in Figure 1. The ethylene glycol is then used to produce ice in an external ice box. Two configurations are applied for the beds, in which the first one uses the aluminum foam structure formed on the external surface of the heat exchanger plain tubes (Al-foam based system), and the second is the classical finned tube form (finned-tube based system). Activated carbon type Maxsorb III in granular form is packed in the aluminum foam structure and in between fins in the finned tube beds. The use of the metal foam structure instead of fins is proposed primarily to enhance the effective thermal conductivity in the adsorbent domain. Aluminum foam is characterized by a lower thermal mass compared to copper foam. Therefore, the former is chosen for the present study as the adsorbent bed is subjected to periodic heating and cooling processes.

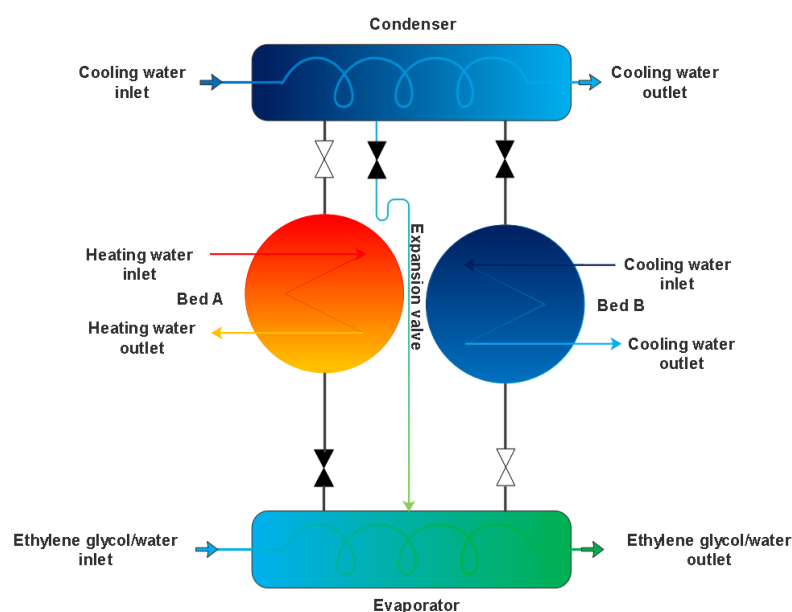


**Figure 1.** Schematic diagram of a two-bed adsorption system used for ice production.

The heating water is supplied to one bed during the regeneration (desorption) process, while the cooling water is supplied to the second bed at the same time to facilitate the adsorption process. Each bed undergoes four consequent processes including preheating, desorption, precooling, and adsorption to perform a complete cycle. More details on the theory of the adsorption refrigeration system can be accessed in reference [35]. Ice can be produced using ethylene glycol, which continuously leaves the evaporator to an external ice production process and returns to enter the evaporator at  $-2\text{ }^{\circ}\text{C}$ .

## 3. Mathematical Modelling

A transient pressure distributed parameter model considering the internal and external mass transfer resistances in the adsorbent domain of an aluminum foamed/finned tube two-bed adsorption system is developed in the current study. Two lumped models of the condenser and evaporator components deeming the heat transfer limits in each component are coupled with the two-bed model at the valve openings as boundary conditions. The coupling of these boundary conditions is switched between the lumped models depending on the mode of operation, in which one bed is connected with the condenser model, and the second is connected with the evaporator model at the same time. During the preheating and precooling modes, the boundaries of the openings are treated as walls.

Figure 2 shows a 2-D axisymmetric design model for the representative adsorber tube containing the four domains: the thermal fluid, plain copper tubes, aluminum foam or

fins packed with activated carbon, and vacuum space. The developed model embraces the volume averaged approach for solving the conservation equations in the porous adsorbent domain. The current model takes into consideration the non-ideal condenser and evaporator pressures by applying their energy balances at the valve opening as boundary conditions. Solving the governing equations simultaneously reveals the capability of the model to detect the local changes of all variables including the pressure, the temperature, and the amount of adsorbate (uptake) within the investigated adsorbent tube. Each adsorbent bed comprises a bundle of tubes, each of which is identical to the adsorbent tube that was used in the simulations. Deducing the overall performance of the system considers the total number of tubes in each bed when connected to the evaporator or the condenser at the four modes of operation. The following assumptions are made in adapting the system of equations used to simulate the adsorption beds:

- Ethanol vapor is considered an ideal gas as it works under a high vacuum pressure.
- The porosities of the metal foam and the adsorbent material are considered isotropic.
- Local thermal equilibrium between the ethanol vapor, adsorbate and adsorbent material.
- No thermal losses from outer surfaces of the reaction beds.

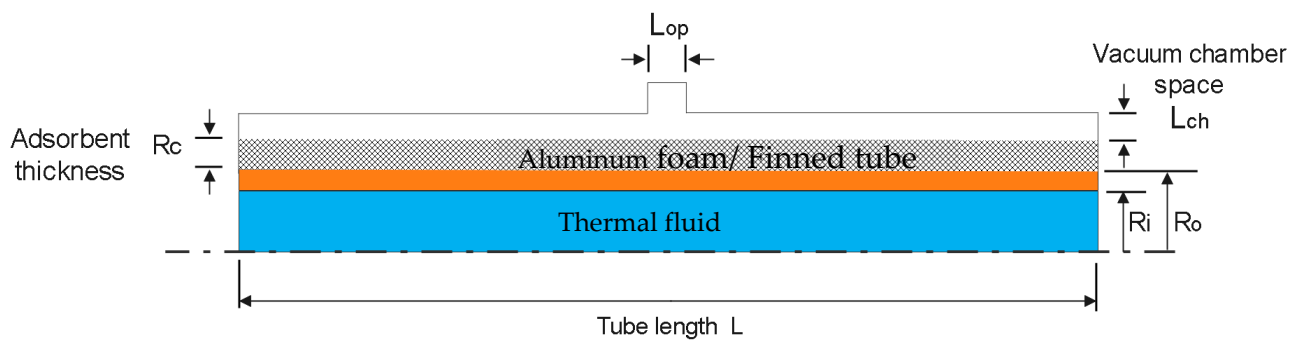


**Figure 2.** The 2-D axisymmetric model of the four investigated domains.

### 3.1. Governing Equations

#### a. Thermal fluid

The liquid water is the thermal fluid flowing inside the copper tubes and used for heating and cooling the beds. A turbulent flow regime for an incompressible fluid is considered, and RANS equations with  $\kappa$ - $\epsilon$  turbulence model are adopted in the modelling as follows:

Mass equation

$$\rho_f \nabla \cdot u_f = 0 \quad (1)$$

Momentum equations

$$\rho_f \frac{\partial u_f}{\partial t} + \rho_f u_f \cdot (\nabla u_f) = -\nabla p I + \nabla \cdot \left[ (\mu + \mu_T) \left( \nabla u_f + (\nabla u_f)^T \right) - \frac{2}{3} \rho_f \kappa I \right] \quad (2)$$

The influence of turbulent flow on the heat transfer propagation inside the tube is imitated in the energy equation using the turbulent thermal conductivity ( $k_T$ ) term and the energy equation can be written as follows [23]:

$$\rho_f C_{p,f} \frac{\partial T_f}{\partial t} + \nabla \cdot (\rho_f C_{p,f} u_f T_f) - \nabla \cdot ((k_f + k_T) \nabla T_f) = 0 \quad (3)$$

#### b. Metal tube and fins

The conservation of energy for the metal tubes and fins domains is only based on the conduction heat transfer mechanism and can be written as:

$$\rho_{met} C_{p,met} \frac{\partial T_{met}}{\partial t} - \nabla \cdot (k_{met} \nabla T_{met}) = 0 \quad (4)$$

### c. Adsorbent domain

Two forms of mass balance equations are employed in the modelling according to the packing configurations of Maxsorb III. [15,36]:

$$\varepsilon_{t,fi} \frac{\partial \rho_v}{\partial t} + (1 - \varepsilon_{t,fi}) \rho_s \frac{\partial X}{\partial t} + \nabla \cdot (\rho_v u) = 0 \quad \text{Finned tube bed} \quad (5)$$

$$\varepsilon_{b,fo} \frac{\partial \rho_v}{\partial t} + (1 - \varepsilon_{t,fo}) \rho_s \frac{\partial X}{\partial t} + \nabla \cdot (\rho_v u) = 0 \quad \text{Al-foam bed} \quad (6)$$

where  $\varepsilon_t$  is the total porosity in the finned tube beds,  $\varepsilon_b$  is the bed porosity in the foamed beds,  $X$  is the instantaneous adsorbate (uptake),  $\rho_v$  is the density of ethanol vapor,  $\rho_s$  is the density of the solid adsorbent and  $u$  is the averaged velocity.

The momentum equations are adapted in the modelling in the two following forms [23]:  
Finned tube bed

$$\frac{\rho_v}{\varepsilon_{t,fi}} \left[ \frac{\partial u}{\partial t} + \frac{1}{\varepsilon_{t,fi}} u \cdot (\nabla u) \right] = \nabla [-pI + \frac{\mu}{\varepsilon_{t,fi}} (\nabla u + (\nabla u)^T) - \frac{2}{3} \frac{\mu}{\varepsilon_{t,fi}} (\nabla \cdot u) I] - \left[ \frac{\mu}{k_{p,fi}} + \frac{Q_m}{\varepsilon_{t,fi}^2} \right] u \quad (7)$$

Al-foam bed

$$\frac{\rho_v}{\varepsilon_{b,fo}} \left[ \frac{\partial u}{\partial t} + \frac{1}{\varepsilon_{b,fo}} u \cdot (\nabla u) \right] = \nabla [-pI + \frac{\mu}{\varepsilon_{b,fo}} (\nabla u + (\nabla u)^T) - \frac{2}{3} \frac{\mu}{\varepsilon_{b,fo}} (\nabla \cdot u) I] - \left[ \frac{\mu}{k_{p,fo}} + \frac{Q_m}{\varepsilon_{b,fo}^2} \right] u \quad (8)$$

$Q_m$  is the source term derived from the mass balance Equations (5) and (6) and can be written as:

$$Q_m = -(1 - \varepsilon_t) \rho_s \frac{\partial X}{\partial t} \quad (9)$$

The energy equation for the adsorbent domain can be expressed as:

$$\frac{\partial}{\partial t} ((\rho C_p) T) + \nabla \cdot (\rho_v u C_{p,v} T) = \nabla \cdot (k \nabla T) + (1 - \varepsilon_t) \rho_s H_{ads} \frac{\partial X}{\partial t} \quad (10)$$

where  $\rho C_p$  is the total thermal capacity of the adsorbent domain, which has two forms according to the activated carbon configuration:

$$\rho C_p = (1 - \varepsilon_{t,fi}) \rho_s (C_{p,s} + X C_{p,a}) + \varepsilon_{t,fi} \rho_v C_{p,v} \quad \text{Finned tube bed} \quad (11)$$

$$\rho C_p = (1 - \varepsilon_{t,fo}) \rho_s (C_{p,s} + X C_{p,a}) + \varepsilon_{b,fo} \rho_v C_{p,v} + \rho_{fo} C_{fo} \quad \text{Al-foam bed} \quad (12)$$

$H_{ads}$  is the isosteric heat of adsorption. The thermal conductivity ( $k$ ) is considered as the bulk thermal conductivity of Maxsorb in the case of the finned tube bed, while  $k$  is the effective thermal conductivity of the foamed packed bed in the case of the aluminum foam bed [15].

### d. Vacuum chamber

Typical mass, momentum, and energy conservation equations for a laminar flow of the ethanol vapor in the vacuum space are employed in the modelling and can be written as follows:

Conservation of mass equation:

$$\frac{\partial \rho_v}{\partial t} + \nabla \cdot (\rho_v u) = 0 \quad (13)$$

Conservation of momentum equations:

$$\rho_v \frac{\partial u}{\partial t} + \rho_v u \cdot \nabla (u) = -\nabla p I + \nabla \cdot \left[ \mu \left( \nabla u + (\nabla u)^T \right) - \frac{2}{3} \mu (\nabla \cdot u) I \right] \quad (14)$$

Conservation of energy equation:

$$\frac{\partial (\rho_v C_{p,v} T_v)}{\partial t} + \nabla \cdot (\rho_v u C_{p,v} T_v) - \nabla \cdot (k_v \nabla T_v) = 0 \quad (15)$$

The vapor pressure in both the adsorbent and the vacuum space domains is related to the vapor temperature and density using the ideal gas state equation.

e. Evaporator model

The evaporator heat balance equation is used to determine the temperature of evaporation, thereby calculating the evaporator pressure. The heat balance equation considers the effect of the evaporator thermal mass and the heat transfer effectiveness  $\varepsilon_{eva}$ , as shown in Equation (16)

$$\begin{aligned} & \left[ M_{eva,rl} C_{p,eva,rl} + M_{eva,met} C_{p,eva,met} \right] \frac{dT_{eva}}{dt} \\ & = \dot{m}_{Eth,Gly} C_{p,Eth,Gly} \varepsilon_{eva} (T_{Eth,Gly,i} - T_{eva}) \\ & - (1 - \alpha) \dot{m}_{v,eva} N_{tube,adsorber} [LH_{eva} - C_{p,rl} (T_{cond} - T_{eva})] \end{aligned} \quad (16)$$

where

$$\varepsilon_{eva} = 1 - \exp \left( \frac{-UA_{eva}}{\dot{m}_{Eth,Gly} C_{p,Eth,Gly}} \right) \quad (17)$$

and  $N_{tube,adsorber}$  is the total number of tubes in the adsorbent bed.

f. Condenser model

Similar to the evaporator modelling, the heat balance equation for the condenser considers the effect of the condenser thermal mass and its thermal effectiveness  $\varepsilon_{cond}$ . Equation (18) is used to determine the ethanol condensing temperature, thus the condenser pressure.

$$\begin{aligned} & \left[ M_{cond,rl} C_{p,cond,rl} + M_{cond,met} C_{p,cond,met} \right] \frac{dT_{cond}}{dt} \\ & = -\dot{m}_{cw} C_{p,cw} \varepsilon_{cond} (T_{cond} - T_{cw,i}) \\ & + (1 - \beta) \dot{m}_{v,cond} N_{tube,adsorber} [LH_{cond} + C_{p,rv} (T_{v,out} - T_{cond})] \end{aligned} \quad (18)$$

where

$$\varepsilon_{cond} = 1 - \exp \left( \frac{-UA_{cond}}{\dot{m}_{cw,cond} C_{p,cw}} \right) \quad (19)$$

and  $\alpha$  and  $\beta$  are flags used to simulate the current states (on/off) of connecting valves that connect the sorption beds with the evaporator and condenser.

g. Adsorption isotherms and kinetics

The linear-driving-force model is defined as a suitable model to represent the resistance to the intraparticle mass transfer [34,37]:

$$\frac{\partial X}{\partial t} = K_{LDF} (X_{eq} - X) \quad (20)$$

where  $K_{LDF}$  is the mass transfer coefficient and can be expressed for the Maxsorb III in the granular form as:

$$K_{LDF} = \mathcal{A} \exp \left( \frac{-E_a}{\mathcal{R}_u T} \right) \quad (21)$$

$A$  is pre-exponential factor,  $\mathcal{R}_u$  is the universal gas constant and  $E_a$  is the activation energy:

For the equilibrium adsorption uptake of Maxsorb III/ethanol ( $X_{eq}$ ) [34,37]

$$X_{eq} = X_{max} \exp \left[ - \left( \frac{RT}{E} \ln \left( \frac{P_s}{p} \right) \right)^n \right] \quad (22)$$

where,  $X_{max}$  is the maximum adsorption uptake,  $\mathcal{R}$  is the gas constant,  $T$  is the adsorbent temperature,  $E$  is the adsorption characteristics parameter,  $n$  is the heterogeneity parameter,  $P$  is local pressure and  $P_s$  is the saturation pressure calculated from Antoine's equation for ethanol by

$$P_s = 0.1333 \times 10^{A - \frac{B}{T+C}} \quad (23)$$

where,  $A$ ,  $B$  and  $C$  are equation constants,  $T$  is the temperature in °C and  $P_s$  is the pressure in kPa.

#### h. Performance indicators

The performance indicators employed in this study to evaluate the adsorption ice production system are defined by the coefficient of performance ( $COP$ ), the specific cooling power ( $SCP$ ), and the daily ice production ( $DIP$ ) as follows:

$$Q_{eva} = \frac{1}{t_{cycle}} \int_0^{t_{cycle}} \dot{m}_{Eth,Gly} C_{Eth,Gly} (T_{Eth,Gly,i} - T_{Eth,Gly,out}) dt \quad (24)$$

$$Q_{heat} = \frac{1}{t_{cycle}} \int_0^{t_{cycle}} \dot{m}_{hw} C_{hw} (T_{hw,i} - T_{hw,out}) dt \quad (25)$$

$$COP = \frac{Q_{eva}}{Q_{heat}} \quad (26)$$

$$SCP = \frac{Q_{eva}}{M_s} \quad (27)$$

$$DIP = \sum_0^N \int_0^{t_{cycle}} \frac{\dot{m}_{Eth,Gly} C_{Eth,Gly} (T_{Eth,Gly,i} - T_{Eth,Gly,out})}{cp_l (T_{w,in} - T_{freezing}) + h_{fg} + cp_{ice} (T_{freezing} - T_{ice,out})} dt \quad (28)$$

where  $M_s$  is adsorbent mass in the two sorption beds and  $N$  is the total cycles in 8 h per day as the system is supposed to be driven by solar energy.

All thermophysical properties, operational parameters, and constant parameters for isotherms used for the simulations are furnished in Table 1. Figure 2 illustrates the simulated bed tube and the four associated domains.

**Table 1.** The main parameters used in the simulations.

Parameter	Value	Unit	Ref.
Activated carbon density ( $\rho_s$ )	2200	kg·m <sup>-3</sup>	[34]
Activated carbon specific heat ( $C_{p,s}$ )	1375	J·kg <sup>-1</sup> ·k <sup>-1</sup>	[34]
Aluminum foam density ( $\rho_{fo}$ )	270	kg·m <sup>-3</sup>	[15]
Aluminum foam specific heat ( $C_{p,fo}$ )	895	J·kg <sup>-1</sup> ·k <sup>-1</sup>	[15]
Bulk density ( $\rho_{bulk}$ )	275	kg·m <sup>-3</sup>	[34]
Bed permeability (Al-foam bed) ( $K_{p,fo}$ )	$3 \times 10^{-12}$	m <sup>2</sup>	[34]
Bed permeability (finned tube bed) ( $K_{p,fi}$ )	$6.296 \times 10^{-12}$	m <sup>2</sup>	[34]
Particle porosity ( $\varepsilon_p$ )	0.789	-	-
Bed porosity (Al-foam bed) ( $\varepsilon_{b,fo}$ )	0.3416	-	-

Table 1. Cont.

Parameter	Value	Unit	Ref.
Bed porosity (finned tube bed) ( $\varepsilon_{b,fi}$ )	0.4075	-	[34]
Total porosity (Al-foam bed) ( $\varepsilon_{t,fo}$ )	0.861	-	-
Total porosity (finned tube bed) ( $\varepsilon_{t,fi}$ )	0.875	-	-
Foam porosity ( $\varepsilon_{fo}$ )	0.9	-	[15,38]
Thermal conductivity of aluminum foam ( $k_{fo}$ )	6	$\text{W}\cdot\text{m}^{-1}\cdot\text{K}^{-1}$	[15,38]
Thermal conductivity of Activated carbon ( $k_{Ac}$ )	0.2	$\text{W}\cdot\text{m}^{-1}\cdot\text{K}^{-1}$	[34]
Pre-exponential factor ( $A$ )	132.89	$\text{s}^{-1}$	[34]
Activation energy ( $E_a$ )	22.97	$\text{kJ}\cdot\text{mol}^{-1}$	[34]
Isosteric heat of adsorption at ( $H_{ads}$ )	1002	$\text{kJ}\cdot\text{kg}^{-1}$	[34]
Maximum uptake ( $X_{max}$ )	1.2	$\text{kg}\cdot\text{kg}^{-1}$	[34]
Adsorption characteristics parameter ( $E$ )	139.5	$\text{kJ}\cdot\text{kg}^{-1}$	[34]
Heterogeneity parameter ( $n$ )	1.8	-	[34]
<b>The geometrical and operating parameters of the beds.</b>			
Tube length ( $L$ )	0.4	m	[23]
Tube inner radius ( $R_i$ )	3.15	mm	[23]
Tube outer radius ( $R_o$ )	3.96	mm	[23]
Fin thickness ( $F_{th}$ )	0.22	mm	[23]
Fin spacing ( $F_{sp}$ )	1 & 2	mm	-
Vacuum chamber space ( $L_{ch}$ )	2	mm	[23]
Heating water mass flowrate ( $\dot{m}_{hw}$ ) (For $N_{tubes} = 309$ per bed)	5.394	$\text{kg}\cdot\text{s}^{-1}$	[23]
Cooling water mass flowrate ( $\dot{m}_{cw,b}$ ) (For $N_{tubes} = 309$ per bed)	7.628	$\text{kg}\cdot\text{s}^{-1}$	[23]
Inlet regeneration water temperature ( $T_{hw,i}$ )	90	$^{\circ}\text{C}$	-
Inlet cooling water temperature ( $T_{cw,i}$ )	25	$^{\circ}\text{C}$	-

### 3.2. Initial and Boundary Conditions

The effect of the initial conditions on the calculated performance indicators is eliminated after six complete cycles when all variables reached cyclic steady-state conditions. The set of boundary conditions employed in the modelling can be written as follows [23]:

Thermal fluid at inlet during preheating and desorption modes

$$T_f \Big|_{z=0} = T_{hw,i}, \quad u_z = u_{ave,hot,in}, \quad u_r = 0$$

Thermal fluid at inlet during precooling and adsorption modes

$$T_f \Big|_{z=0} = T_{cw,i}, \quad u_z = u_{ave,cool,in}, \quad u_r = 0$$

Thermal fluid at outlet

$$\frac{\partial T_f}{\partial z} \Big|_{z=L} = 0, \quad p_f = P_{atm}$$

Valve opening during the desorption mode

$$\frac{\partial T}{\partial r} = 0, \quad p = P_{cond}$$

Valve opening during the adsorption mode

$$T_v = T_{eva}, \quad p = P_{eva}$$

The parameters used for the condenser and evaporator models are furnished in Table 2.

**Table 2.** The adopted parameters for the condenser and evaporator in the simulations.

Symbols	Value	Unit
Condenser parameters		
$M_{cond,rl}C_{p,cond,rl} + M_{cond,met}C_{p,cond,met}$	$2.5 \times 4180 + 12 \times 386$	$J \cdot K^{-1}$
$UA_{cond}$	$4114 \times 1.855$	$W \cdot K^{-1}$
$\dot{m}_{cw}C_{p,cw}$	$0.6271 \times 4180$	$W \cdot K^{-1}$
$T_{cw,i}$	25	$^{\circ}C$
Condenser initial temperature ( $T_{cond,init}$ )	25	$^{\circ}C$
Evaporator parameter		
$M_{eva,rl}C_{p,eva,rl} + M_{eva,met}C_{p,eva,met}$	$20 \times 3574.3 + 4.45 \times 386$	$J \cdot K^{-1}$
$UA_{eva}$	$2557 \times 0.6$	$W \cdot K^{-1}$
$\dot{m}_{Eth,Gly}C_{p,Eth,Gly}$	$0.4240225 \times 3574.3$	$W \cdot K^{-1}$
$T_{chw,i}$	-2	$^{\circ}C$
Evaporator initial temperature ( $T_{evap,init}$ )	-2	$^{\circ}C$

### 3.3. Numerical Procedure

The described mathematical model was built in COMSOL Multiphysics by combining six physics to model all the governing equations simultaneously. For the propagation of heat throughout all the physical domains, Heat Transfer Physics was used. The turbulent flow inside the tubes of the sorption beds was modelled through Turbulent Flow ( $k - \epsilon$ ) Physics. Furthermore, Free and Porous Media Flow Physics was involved to represent the mass and the momentum transports in the adsorbent and the vacuum domains, especially for handling the interface between those domains. Additionally, Convection–Diffusion Equation Physics for the LDF model was employed. Finally, two Ordinary Differential Equations were correlated to the system of equations to replicate the evaporator and the condenser pressures at the valve opening. User-defined functions were implemented with the six physics to represent all the source terms. In the solver, a time-dependent study was adopted using the segregated approach while setting MUMPS and PARDISO solvers for best convergence. The time step was set to 0.001 s for preheating and precooling processes, and 1 s for desorption and adsorption processes, to accurately catch the changes of the resolved variables. The Grid Convergence Index (GCI) was calculated for the COP and SCP as main output parameters to verify grid independency of the present study using three options including different numbers and sizes of mesh elements. The GCI values were 0.62% and 0.58% for COP and SCP, respectively. The calculation of GCI followed the same procedures that were discussed by Sosnowski in reference [39]. The maximum change in both COP and SCP was 0.14%. The average mesh element quality was 0.8591 and the maximum growth rates for the boundary mesh elements were 1.08 and 1.1 in the thermal fluid domain, and the adsorbent and vacuum chamber domains, respectively. Therefore, a grid-independent study was established, and the extra-fine choice with about 500,000 mesh elements was selected.

### 3.4. Validation

The validity of the present numerical model was previously confirmed based on the comparison with the experimental works in references [23,40]. Additionally, Figure 3 shows the comparison between the results of the present model with data published by Pinheiro et al. [11] for two adsorbent materials, CPO-27(Ni) and SAPO-34, coated on copper-foam based beds. Very good agreements can be observed between the current model results and the published data.

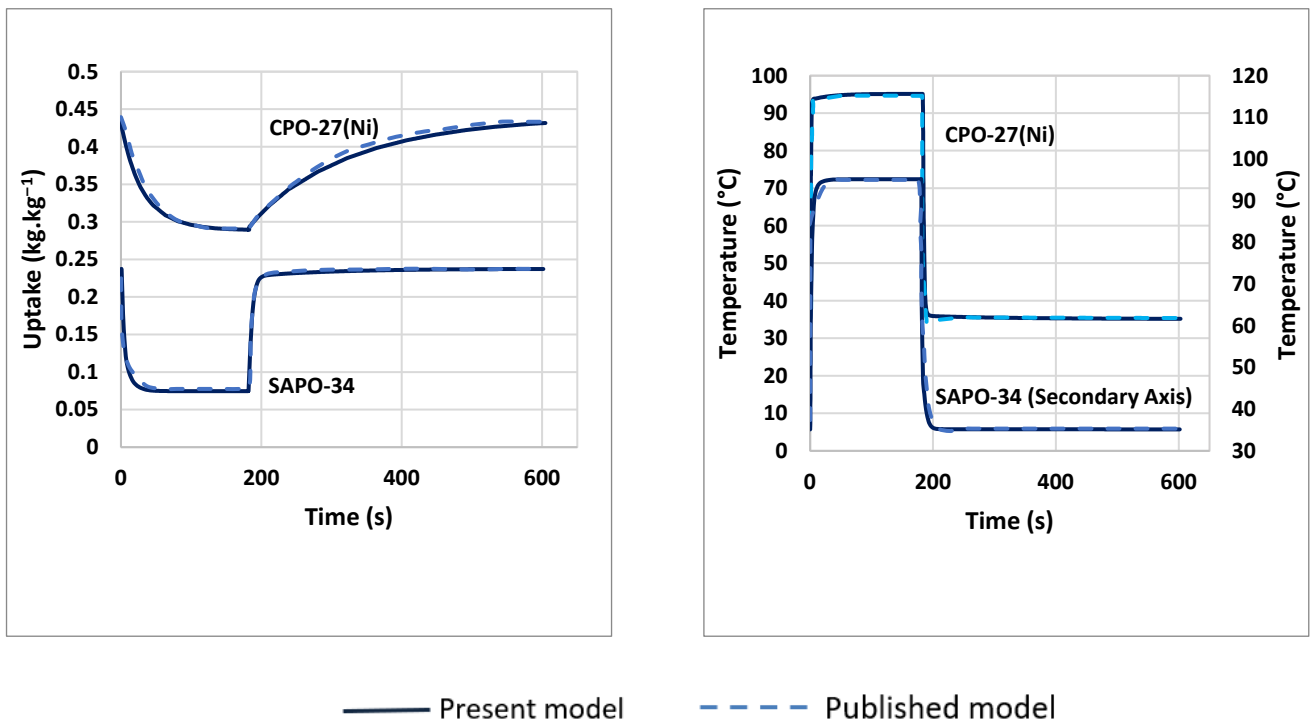


**Figure 3.** The uptake and temperature temporal variations for CPO-27(Ni) and SAPO-34 adsorbent materials obtained from the present model and reference [11].

#### 4. Results and Discussion

The enhancement in the performance of the two-bed adsorption ice production system incorporated foamed beds was investigated by the comparison with the base model of finned tube adsorbent beds at different foam thicknesses/fin heights of 2, 5, and 10 mm and cycle times of 400, 600, 800, 1200 s. In all investigated cases, the total adsorbent mass was kept at 4 kg and 3.8 kg for the finned-tube based system and the Al-foam-based system, respectively, as the Al-foam structure occupied more volume at the same space compared to the fins. This kept identical overall dimensions for both systems at each foam thickness/fin height. The total number of tubes in each bed was set to 309, 95, and 34 at 2 mm, 5 mm, and 10 mm foam thicknesses/fin heights, respectively.

##### 4.1. Numerical Simulation

Spatial and temporal variations of the temperature and uptake during the first 90 s of the adsorption process for the bed modelled tube are shown in Figure 4 for finned-tube and Al-foam beds. The numerical simulation is shown for a 5 mm fin height/foam thickness and cycle time of 400 s. At the starting time of 0 s, the bed just finished the precooling process, and the tube starts to receive the vapor from the evaporator at the valve opening boundary condition. The role of fins and aluminum foam in intensifying the heat transfer within the adsorbent domain is shown in Figure 4a,b. It can be deduced that a more effective decrease in the bed temperature directly increases the bed uptake and improves the system performance. In detail, the average temperature of the adsorbent domain at 90 s is 26.67 °C for the finned-tube bed compared to 31.21 °C for the Al-foam bed, resulting in an average uptake of 0.363 kg/kg and 0.332 kg/kg for the finned-tube bed and Al-foam bed, respectively. Consequently, and after completing the cycle of 400 s, the DIP of the finned-tube based system and Al-foam based system attained 114.3 and 110 kg<sub>ice</sub>·day<sup>-1</sup>, respectively. The increase in the DIP of the finned-tube based system over the Al-foam based one was attributed to the lower bed temperature in the former system during the adsorption process in the given case. The net effects of fin height and spacing against the

foam thickness at different cycle times on the overall performance of the adsorption ice production system will be discussed in the next sections.

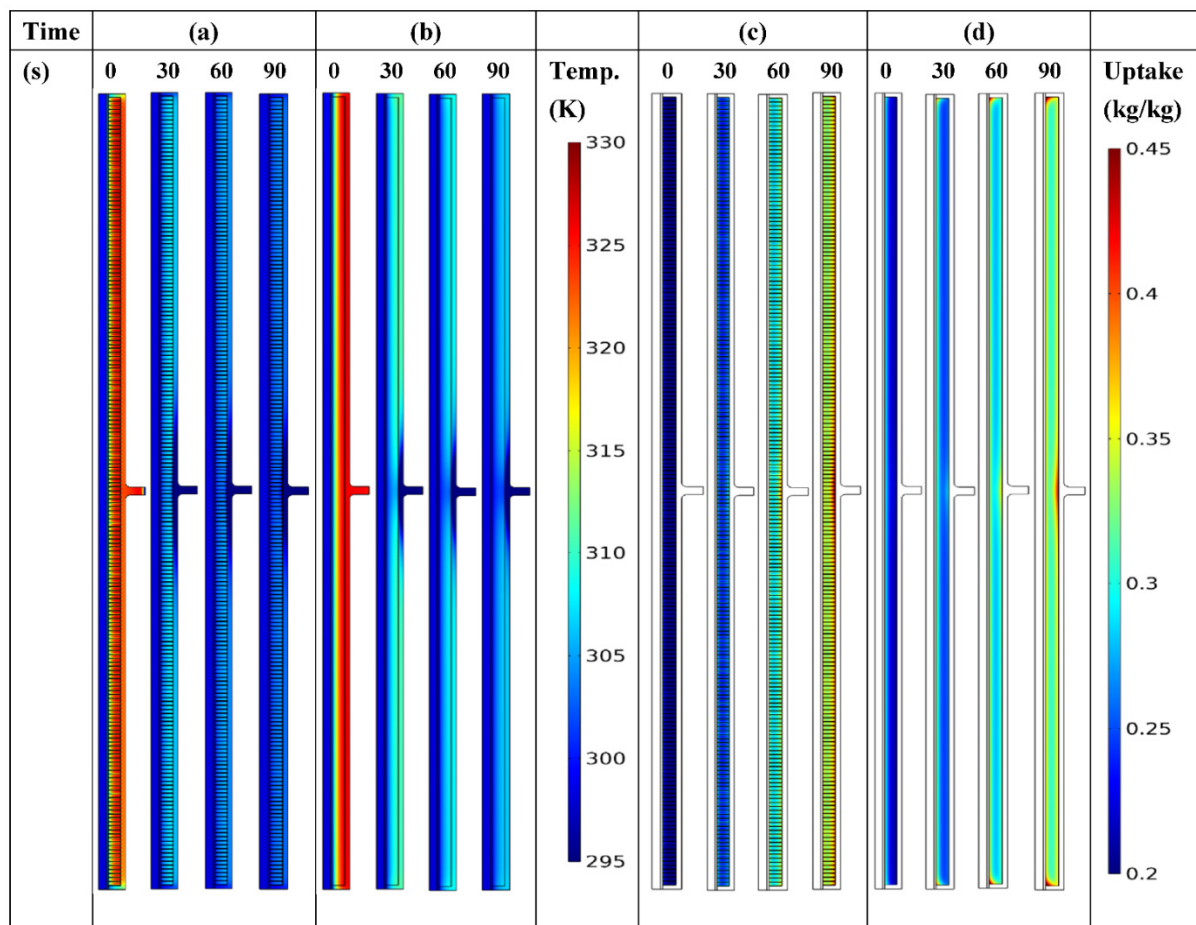


**Figure 4.** Numerical simulations for the spatial variations during the first 90 s of the adsorption: (a,c) the temperature and uptake for the finned tube bed, (b,d) the temperature and uptake for the aluminum foam bed.

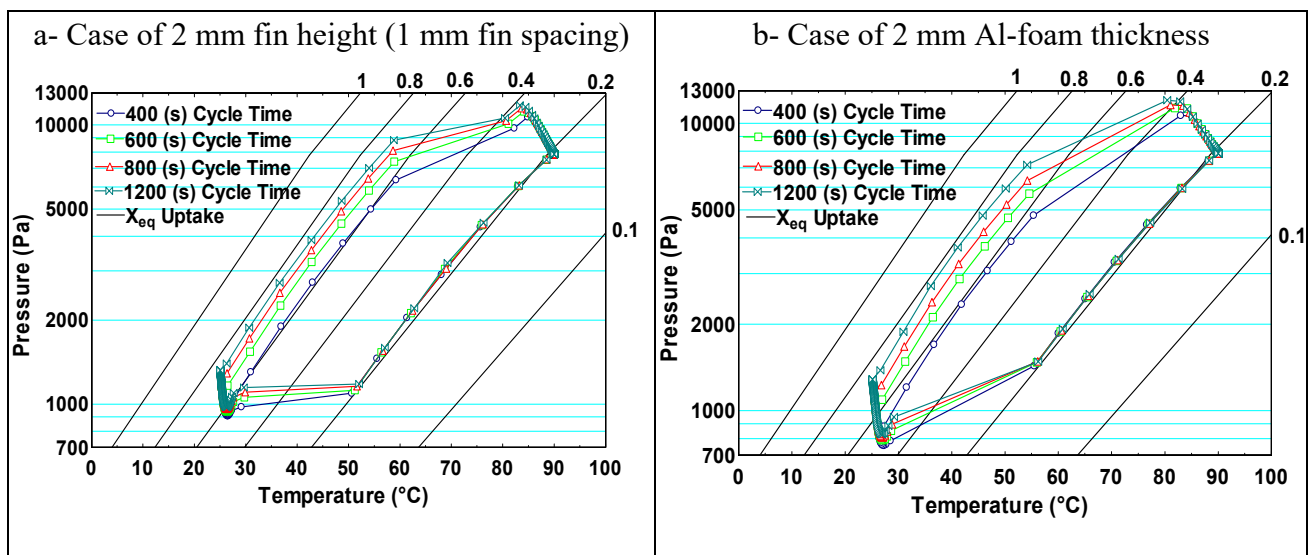
#### 4.2. Effect of Using Fin Height/Foam Thickness of 2 mm

Table 3 shows how the absolute values of the performance indicators are affected by the change in the cycle times. The fin spacing of 1 mm and 2 mm were used for 2 mm fin height in the finned-tube based system. In the case of shorter fin height, all performance indicators improved when the fin spacing changed from 1 mm to 2 mm at each specific cycle time. For both fin spacings, extending the cycle time from 400 s to 1200 s enhanced the COPs by 32% and 35% in the cases of 1- and 2-mm fin spacings, respectively. This is due to the reduction in the sensible heating share with a higher cycle time. However, resulting lower adsorption rates at higher cycle times reduced considerably both SCPs and DIPs. The DIP reduced by 53% and 50% when the cycle time was extended from 400 s to 1200 s, for 1- and 2-mm fin spacings, respectively.

**Table 3.** The performance indicators of the finned-tube base model at 2 mm fin height.

Cycle Time (s)	Case of 1 mm Fin Spacing			Case of 2 mm Fin Spacing		
	COP	SCP $W \cdot kg^{-1}$	DIP $kg_{ice} \cdot day^{-1}$	COP	SCP $W \cdot kg^{-1}$	DIP $kg_{ice} \cdot day^{-1}$
400	0.152	548.2	148.6	0.173	567.5	154.2
600	0.158	436.7	118.5	0.203	465.7	126.3
800	0.185	358.8	97.3	0.219	386.4	104.8
1200	0.201	258.2	70.2	0.233	281.8	76.4

The effects of different cycle times on the average bed temperature, pressure, and uptake during the four processes after reaching cyclic steady-state conditions are shown in Figure 5 for both systems at 2 mm fin height/foam thickness. It can be deduced that increasing the cycle time increases the effective uptake (the difference between the lower and higher uptakes) for both systems by allowing longer time periods for adsorption and desorption processes, while it was slightly more pronounced in the Al-foam based system. The beds in the Al-foam based system attained lower pressures compared to those in the finned-tube based system. This positively affected the system performance by reducing the temperature of the ethylene glycol/water leaving the evaporator.

**Figure 5.** The T-P-X diagram for the bed of both systems during the cyclic steady state at different cycle times and 2 mm fin height/foam thickness. (a) Finned-tube based bed, (b) Al-foam based bed.

The net effects of changing the cycle time on the percentage change of the COPs and DIPs of the Al-foam two-bed system compared with those resulting from the finned-tube based system are shown in Figure 6. It is clearly seen that the Al-foam based system outperformed the finned-tube based system in both COPs and DIPs at different cycle times and both fin spacings of 1 mm and 2 mm. This was attributed to the lower temperature of the ethylene glycol/water leaving the evaporator and the lower adsorbent mass associated with the Al-foam based system, compared with those associated with the finned-tube based system for the given cases.

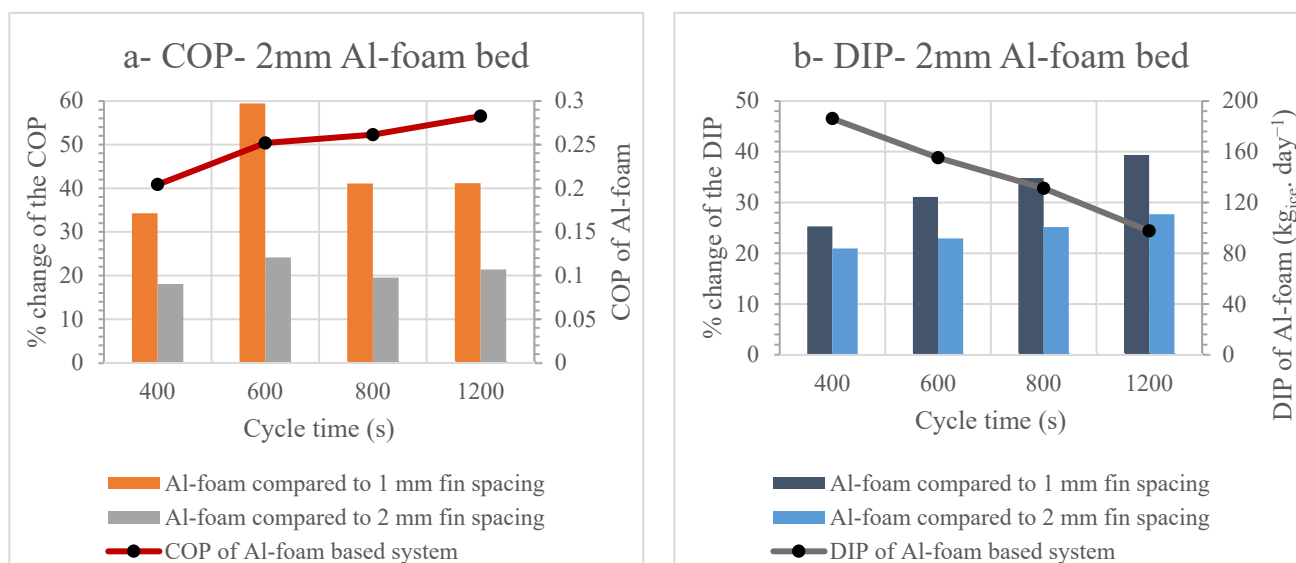


**Figure 6.** Effect of the cycle time on the percentage change in the system COP and DIP when using Al-foam bed with 2 mm thickness. (a) COP, (b) DIP.

The maximum increase in the COP of the Al-foam based system reached 59.4% at a cycle time of 600 s, while the DIP of the Al-foam based system reached its maximum percentage increase of 39.3% at a cycle time of 1200 s, compared with the finned-tube based system with 1 mm fin spacing. Moreover, Figure 6 shows how the COP and DIP of the Al-foam based system was affected by changing the cycle time. Increasing the cycle time enhanced the system COP but reduced the DIP at the given short foam height of 2 mm. This was attributed to the lower rate of adsorption with increasing time as the uptake approaches its upper limit in the given condition. It is important to mention that the Al-foam based system at a cycle time of 400 s can produce ice at a maximum of  $186.2 \text{ kg}_{\text{ice}} \cdot \text{day}^{-1}$  with the system COP at 0.204, while extending the cycle time to 1200 s can considerably reduce the DIP to  $97.8 \text{ kg}_{\text{ice}} \cdot \text{day}^{-1}$  with an enhancement in the system COP to 0.284.

#### 4.3. Effect of Using Fin Height/Foam Thickness of 5 mm

The absolute values of the COP, SCP, and DIP resulting from the finned-tube based system at 5 mm fin height are depicted in Table 4 for 1 mm and 2 mm fin spacings. Compared to the 2 mm fin height, Table 3, the system COP was enhanced noticeably with increasing the fin height to 5 mm and this was more pronounced at 2 mm fin spacing. However, the system SCP and DIP were affected negatively by increasing the fin height from 2 mm to 5 mm. For example, DIPs were reduced by 20.6% and 3.6% at cycle times of 400 s and 1200 s, respectively. This was a direct result of the reduction in the effective uptakes that can be noticed when comparing Figures 5a and 7a.

**Table 4.** The performance indicators of the finned-tube base model at 5 mm fin height.

Cycle Time (s)	Case of 1 mm Fin Spacing			Case of 2 mm Fin Spacing		
	COP	SCP W·kg <sup>-1</sup>	DIP kg <sub>ice</sub> ·day <sup>-1</sup>	COP	SCP W·kg <sup>-1</sup>	DIP kg <sub>ice</sub> ·day <sup>-1</sup>
400	0.213	435	118	0.237	421.6	114.4
600	0.277	380	103	0.293	385	104.45
800	0.278	325.5	88.3	0.318	340.3	92.3
1200	0.289	249.7	67.7	0.344	266.8	72.36

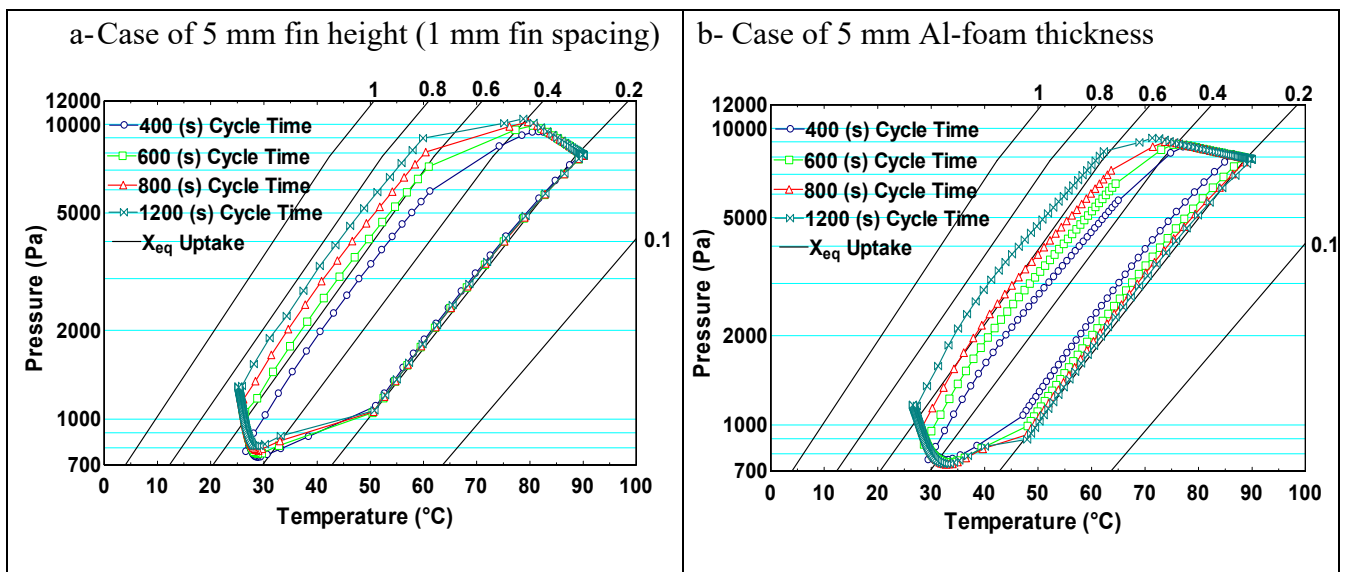


**Figure 7.** The T-P-X diagram for the bed of both systems during the cyclic steady state at different cycle times and 5 mm fin height/foam thickness. (a) Finned-tube based bed, (b) Al-foam based bed.

At a cycle time of 400 s, the effective uptake in the foamed bed was much lower than that attained by the finned-tube bed, as can be shown by comparing Figure 7a,b, for 5 mm fin height/foam thickness. Increasing the cycle time enhanced considerably both beds' uptake at the end of the adsorption process. In the foamed bed, the lower limit of the uptake at the end of the desorption process decreased with increasing the cycle time and reached about 0.2 kg/kg at a cycle time of 1200 s. This affected positively the performance of the Al-foam based system for the higher cycle time.

The net effects of changing the cycle time on the percentage change in the COP and DIP of the adsorption system when fixing the fin height/foam thickness at 5 mm are shown in Figure 8. The COPs of the Al-foam based system outperformed those of the finned-tube based system with 1 mm fin spacing at all cycle times. The maximum increase of the COP was 26.7% at 1200 s. However, using the foamed beds to enhance the COP compared to the finned-tube based system with 2 mm fin spacing can only be achieved at higher cycle times of 800 s (2.3% increase) and 1200 s (6.8% increase), as shown in Figure 8a.

Working at higher cycle times of 800 s and 1200 s can also enhance the DIPs of the Al-foam based system over those of the finned-tube based system with both 1- and 2-mm fin spacings. The maximum increase of only 16.8% (which was 39.3% at 2 mm foam thickness, Figure 6b in the DIP of the Al-foam based system was attained at a cycle time of 1200 s and 5 mm foam thickness, as shown in Figure 8b. This was due to the negative effect of using less adsorbent mass in the foamed beds compared to the finned-tube beds, which was not compensated by higher heat and mass transfer enhancement as in the case of 2 mm foam thickness. Additionally, the performance of the Al-foam based system was affected more negatively by the reduction of the total number of tubes used in each bed (the total number was reduced from 309 to 95 tubes). The reduction in the number of tubes leads to a reduction in cooling and heating mass flow rates in the case of 5 mm foam thickness.

Using a foam thickness of 5 mm was better in terms of the system COP compared to 2 mm foam thickness at each cycle time. The maximum COP of 0.366 for the Al-foam based system was attained at a cycle time of 1200 s, as shown in Figure 8. On the other hand, the DIP was reduced by 20.1% (from 99.1 to 79.1 kg<sub>ice</sub>·day<sup>-1</sup>) when changing the cycle time from 400 s to 1200 s, compared to a 47.5% reduction (from 186.2 to 97.6 kg<sub>ice</sub>·day<sup>-1</sup>) in the same case with 2 mm foam thickness.

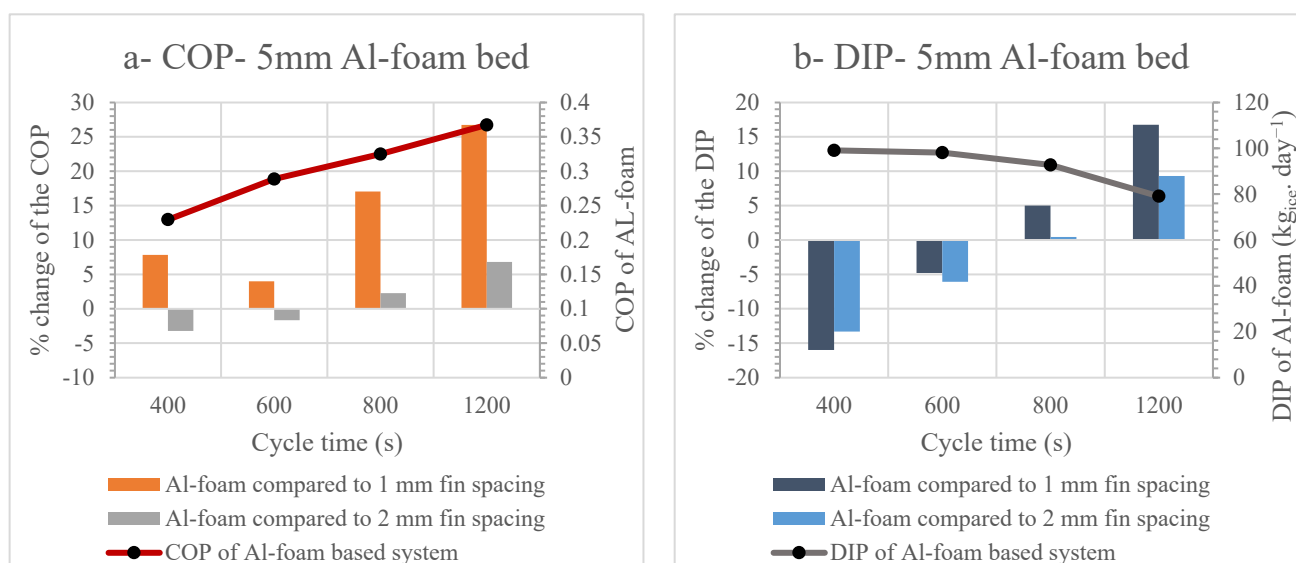


**Figure 8.** Effect of the cycle time on the percentage change in the system COP and DIP when using Al-foam bed with 5 mm thickness. (a) COP, (b) DIP.

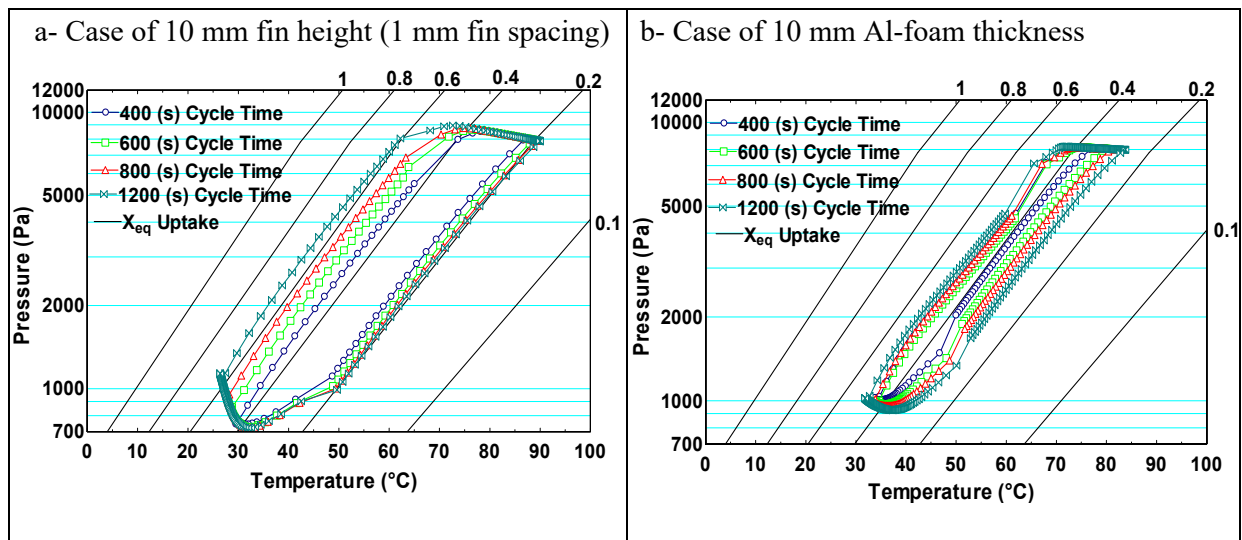
#### 4.4. Effect of Using Fin Height and Foam Thickness of 10 mm

Increasing the fin height from 5 mm to 10 mm enhanced the COP of the finned-tube two-bed adsorption ice production system at only a longer cycle time, as can be deduced from the comparison between Tables 4 and 5. The COP increased by 13.8% when the fin height of 10 mm replaced that of 5 mm at 1mm fin spacing and 1200 s cycle time. The maximum COP of 0.37 was attained at a cycle time of 1200 s with 2 mm fin spacing. However, both the SCP and DIP were reduced considerably by 43.3% at a shorter cycle time of 400 s when using a 10 mm fin height instead of 5 mm.

**Table 5.** The performance indicators of the finned-tube base model at 10 mm fin height.

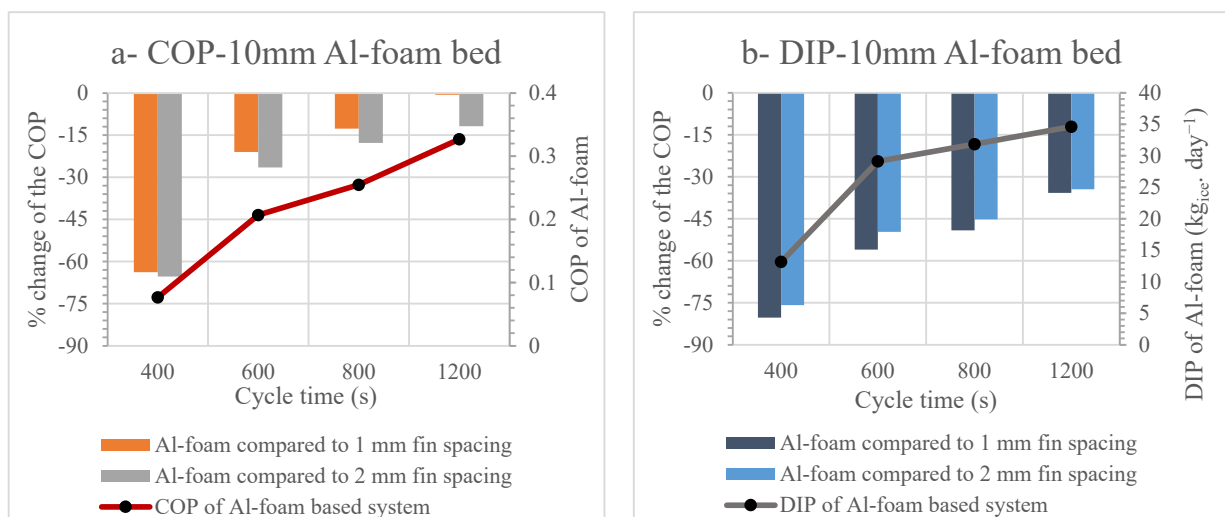
Cycle Time (s)	Case of 1 mm Fin Spacing			Case of 2 mm Fin Spacing		
	COP	SCP $W \cdot kg^{-1}$	DIP $kg_{ice} \cdot day^{-1}$	COP	SCP $W \cdot kg^{-1}$	DIP $kg_{ice} \cdot day^{-1}$
400	0.212	246.6	66.8	0.221	200.7	54.4
600	0.262	244.3	66.3	0.282	213.4	57.9
800	0.292	230.8	62.6	0.31	214.3	58.2
1200	0.329	198.7	53.8	0.37	194.9	53.1

Figure 9 illustrates how the average effective uptake, pressure, and temperature in the adsorbent domain were significantly changed while simulating the two beds of each configuration in two identical systems with 10 mm fin height/foam thickness. The effective uptake of the Al-foam based bed was reduced dramatically compared with that of the finned-tube based bed at all cycle times and worsened at shorter cycle times. The smaller number of adsorbers' tubes used with 10 mm fin height/foam thickness (34 tubes in each bed) negatively affected the effective uptake in the Al-foam based system to a much greater degree than in the finned-tube one. This was attributed to the lower permeability in the adsorbent domain of the foamed bed, which was one-half less than that in the finned bed system, recalling that the effect of the permeability increases with a higher foam thickness. Consequently, the increase of the mass transfer resistance demolished the enhancement in the heat transfer through the foamed adsorbent bed.



**Figure 9.** The T-P-X diagram for the bed of both systems during the cyclic steady state at different cycle times and 10 mm fin height/foam thickness. (a) Finned-tube based bed, (b) Al-foam based bed.

Figure 10 demonstrates the net effect of changing the cycle time using 10 mm foam thickness compared with the finned tube bed of 10 fin height on the COP and DIP of the two-bed adsorption ice maker. The COP and DIP of the Al-foam based system were reduced dramatically when a higher foam thickness of 10 mm was employed. The system COP and DIP were reduced by 63.8% and 75.8% at a cycle time of 400 s, while they were reduced by 1% and 35.8% at a cycle time of 1200 s, respectively, compared with the base model of 1 mm fin spacing.



**Figure 10.** Effect of the cycle time on the percentage change in the system COP and DIP when using Al-foam bed with 10 mm thickness. (a) COP, (b) DIP.

Increasing the cycle time from 400 s to 1200 s in the case of the Al-foam based system enhanced considerably both COP and DIP as they increased by 326% and 163%, respectively. Using the higher foam thickness of 10 mm should be associated with higher cycle time, which needs more investigation in future work as a small number of tubes in the adsorbent bed could be preferred to reduce the circulated heating and cooling water flow rates in a certain application. In addition, an adsorbent bed with ethanol refrigerant in adsorption ice production systems works under very high vacuum pressures, which makes the mass transfer mechanisms in the adsorbent domain play a critical role. In such a case, increasing

the permeability of the foamed adsorbent bed is a crucial requirement to enhance the performance of Al-foam based adsorption ice production systems compared to the finned-tube one.

## 5. Conclusions

The present research is considered an attempt to explore the potential of using aluminum foam in contrast to the classical packing method using finned tubes in the adsorbent bed of an adsorption ice production system. A fully coupled numerical model was developed to investigate the effect of changing the cycle time along with different foam thicknesses/fin heights on the performance of both Al-foam and finned-tube based systems. The main outcomes can be summarized as follows:

- The study reveals the superiority of Al-foam based systems in ice production at relatively smaller thickness of the foam. At 2 mm foam thickness, the maximum increase in the COP was 59.4% (with a 31.1% increase in the DIP) at a cycle time of 600 s, while the maximum increase in the DIP was 39.3% (with a 41.2% increase in the COP), compared to the finned-tube based system.
- The best energy conversion was attained at a 5 mm foam thickness with a COP of 0.366 and associated DIP of 79 kg<sub>ice</sub>·day<sup>-1</sup> at a cycle time of 600 s. Thus, this foam thickness and cycle time could be chosen when thermal energy sources are limited.
- Increasing the foam thickness to 10 mm deteriorated the performance of the Al-foam based system due to the dramatic decrease in the effective uptake resulting from the increase of the intraparticle mass transfer resistance. Although the increase in the foam thickness apparently can reduce the number of tubes by accommodating much more adsorbent material, further investigation is needed to compromise between the size of the heat exchanger and the effective permeability of larger thicknesses.
- The shorter the cycle time, the more the ice production rate and the better the specific cooling power. Although the COP will be worse at lower cycle times, the implementation of low-grade thermal waste heat or solar heating collectors to drive such adsorption systems makes it reliable and competitive to electrical driven ice production systems.

**Author Contributions:** Conceptualization, M.B.E.; data curation, J.O. and A.E.-L.; formal analysis, H.A.-A. and A.E.-L.; funding acquisition, H.A.-A.; investigation, M.B.E., M.S.E., J.O. and A.E.-L.; methodology, M.B.E. and O.E.; project administration, H.A.-A.; software, M.B.E., M.S.E. and O.E.; supervision, H.A.-A.; validation, J.O. and A.E.-L.; visualization, O.E.; writing—original draft, M.S.E.; writing—review and editing, M.B.E. All authors have read and agreed to the published version of the manuscript.

**Funding:** This Project was funded by the National Plan for Science, Technology and Innovation (MAARIFAH), King Abdulaziz City for Science and Technology, Kingdom of Saudi Arabia, Award Number (II-ENE1845-02).

**Institutional Review Board Statement:** Not applicable.

**Informed Consent Statement:** Not applicable.

**Conflicts of Interest:** The authors declare that they have no known competing financial interests or personal relationships that could have appeared to influence the work reported in this paper.

## Nomenclature

<i>COP</i>	Coefficient of performance (–)
<i>C<sub>p</sub></i>	Specific heat capacity (J·kg <sup>-1</sup> ·K <sup>-1</sup> )
<i>D<sub>s</sub></i>	Surface diffusivity (m <sup>2</sup> ·s <sup>-1</sup> )
<i>D<sub>so</sub></i>	Pre-exponent constant of surface diffusivity (m <sup>2</sup> ·s <sup>-1</sup> )
<i>DIP</i>	Daily ice production (kg·day <sup>-1</sup> )
<i>E<sub>a</sub></i>	Activation energy of surface diffusion (J·mol <sup>-1</sup> )

$k$	Thermal conductivity ( $\text{W}\cdot\text{m}^{-1}\cdot\text{K}^{-1}$ )
$k_T$	Turbulent thermal conductivity ( $\text{W}\cdot\text{m}^{-1}\cdot\text{K}^{-1}$ )
$k_p$	Bed permeability ( $\text{m}^2$ )
$K_{LDF}$	Mass transfer coefficient ( $\text{s}^{-1}$ )
$LH$	Latent heat ( $\text{J}\cdot\text{kg}^{-1}$ )
$M$	Mass (kg)
$N$	Number of cycles per day
$p$	Pressure (Pa)
$Q_m$	Source term in mass balance equation ( $\text{m}^2$ )
$Q_{ads}$	Isosteric heat of adsorption at half coverage ( $\text{J}\cdot\text{kg}^{-1}$ )
$\mathcal{R}$	Specific gas constant ( $\text{J}\cdot\text{kg}^{-1}\cdot\text{K}^{-1}$ )
$\mathcal{R}_u$	Universal gas constant ( $\text{J}\cdot\text{mol}^{-1}\cdot\text{K}^{-1}$ )
$R$	Radius (m)
$SCP$	Specific cooling power ( $\text{W}\cdot\text{kg}^{-1}$ )
$T$	Temperature (K)
$t$	Time (s)
$UA$	Heat transfer conductance ( $\text{W}\cdot\text{K}^{-1}$ )
$u$	Fluid velocity ( $\text{m}\cdot\text{s}^{-1}$ )
$X$	Uptake ( $\text{kg}_{\text{ref}}\cdot\text{kg}_{\text{ad}}^{-1}$ )
$X_{eq}$	Equilibrium adsorption uptake ( $\text{kg}_{\text{ref}}\cdot\text{kg}_{\text{ad}}^{-1}$ )

Greek symbols:

$\rho$	Density ( $\text{kg}\cdot\text{m}^{-3}$ )
$\mu$	Dynamic viscosity (Pa·s)
$\mu^T$	Turbulent dynamic viscosity (Pa·s)
$\varepsilon_p$	Particle porosity (–)
$\varepsilon_b$	Bed porosity (–)
$\varepsilon_{fo}$	Foam porosity (–)
$\varepsilon$	Effectiveness (–)

Subscripts and superscripts:

$ads$	Adsorbent
$a$	Adsorbate
$b$	Bed
$cw$	Cooling water
$cond$	Condenser
$comp$	Composite
$Eth, Gly$	Ethylene Glycol
$eva$	Evaporator
$eq$	Equilibrium
$f$	Fluid
$fo$	Foam
$fi$	Finned
$hw$	Heating water
$i$	Inlet
$init$	Initial
$LDF$	Linear driving Force
$met$	Metal
$out$	Outlet
$rl$	Refrigerant liquid
$rv$	Refrigerant Vapor
$s$	Solid Adsorbent
$sat$	Saturation
$t$	Total
$v$	Vapor
$w$	Water

## References

1. Qasem, N.A.; El-Shaarawi, M.A. Improving ice productivity and performance for an activated carbon/methanol solar adsorption ice-maker. *Sol. Energy* **2013**, *98*, 523–542. [[CrossRef](#)]
2. Sah, R.P.; Choudhury, B.; Das, R.K. A review on low grade heat powered adsorption cooling systems for ice production. *Renew. Sustain. Energy Rev.* **2016**, *62*, 109–120. [[CrossRef](#)]
3. Islam, M.P.; Morimoto, T. Thermodynamic performances of a solar driven adsorption system. *Sol. Energy* **2016**, *139*, 266–277. [[CrossRef](#)]
4. Luberti, M.; Di Santis, C.; Santori, G. Ammonia/Ethanol Mixture for Adsorption Refrigeration. *Energies* **2020**, *13*, 983. [[CrossRef](#)]
5. Hassan, A.A.; Elwardany, A.E.; Ookawara, S.; El-Sharkawy, I.I. Performance investigation of integrated PVT/adsorption cooling system under the climate conditions of Middle East. *Energy Rep.* **2020**, *6*, 168–173. [[CrossRef](#)]
6. Mikšik, F.; Miyazaki, T.; Thu, K.; Miyawaki, J.; Nakabayashi, K.; Wijayanta, A.T.; Rahmawati, F. Enhancing water adsorption capacity of acorn nutshell based activated carbon for adsorption thermal energy storage application. *Energy Rep.* **2020**, *6*, 255–263. [[CrossRef](#)]
7. Alvarez, J.C.; Bravo, L.; Marçal, R.C.; Hatakeyama, K.; Barrantes, E. Knowledge construction and systematization of solar adsorption refrigeration prototypes. *Energy Rep.* **2021**, *7*, 428–440. [[CrossRef](#)]
8. Teo, H.W.B.; Chakraborty, A.; Kitagawa, Y.; Kayal, S. Experimental study of isotherms and kinetics for adsorption of water on Aluminium Fumarate. *Int. J. Heat Mass Transf.* **2017**, *114*, 621–627. [[CrossRef](#)]
9. Hassan, H.Z. Performance Evaluation of a Continuous Operation Adsorption Chiller Powered by Solar Energy Using Silica Gel and Water as the Working Pair. *Energies* **2014**, *7*, 6382–6400. [[CrossRef](#)]
10. Freni, A.; Bonaccorsi, L.; Proverbio, E.; Maggio, G.; Restuccia, G. Zeolite synthesised on copper foam for adsorption chillers: A mathematical model. *Microporous Mesoporous Mater.* **2009**, *120*, 402–409. [[CrossRef](#)]
11. Pinheiro, J.M.; Salústio, S.; Geraldes, V.; Valente, A.A.; Silva, C.M. Copper foam coated with CPO-27(Ni) metal-organic framework for adsorption heat pump: Simulation study using OpenFOAM. *Appl. Therm. Eng.* **2020**, *178*, 115498. [[CrossRef](#)]
12. Xu, Z.; Yin, Y.; Shao, J.; Liu, Y.; Zhang, L.; Cui, Q.; Wang, H. Study on heat transfer and cooling performance of copper foams cured MIL-101 adsorption unit tube. *Energy* **2020**, *191*, 116302. [[CrossRef](#)]
13. Schnabel, L.; Tatlier, M.; Schmidt, F.; Erdem-Şenatalar, A. Adsorption kinetics of zeolite coatings directly crystallized on metal supports for heat pump applications (adsorption kinetics of zeolite coatings). *Appl. Therm. Eng.* **2010**, *30*, 1409–1416. [[CrossRef](#)]
14. Calabrese, L.; Bonaccorsi, L.; Bruzzaniti, P.; Frazzica, A.; Freni, A.; Proverbio, E. Adsorption performance and thermodynamic analysis of SAPO-34 silicone composite foams for adsorption heat pump applications. *Mater. Renew. Sustain. Energy* **2018**, *7*, 24. [[CrossRef](#)]
15. Mohammed, R.H.; Mesalhy, O.; Elsayed, M.L.; Chow, L.C. Performance enhancement of adsorption beds with silica-gel particles packed in aluminum foams. *Int. J. Refrig.* **2019**, *104*, 201–212. [[CrossRef](#)]
16. Hu, P.; Yao, J.-J.; Chen, Z.-S. Analysis for composite zeolite/foam aluminum–water mass recovery adsorption refrigeration system driven by engine exhaust heat. *Energy Convers. Manag.* **2009**, *50*, 255–261. [[CrossRef](#)]
17. Jing, H.; Exell, R. Simulation and sensitivity analysis of an intermittent solar-powered charcoal/methanol refrigerator. *Renew. Energy* **1994**, *4*, 133–149. [[CrossRef](#)]
18. Dakkama, H.J.; Youssef, P.G.; Al-Dadah, R.K.; Mahmoud, S. Adsorption ice making and water desalination system using metal organic frameworks/water pair. *Energy Convers. Manag.* **2017**, *142*, 53–61. [[CrossRef](#)]
19. Hassan, H.; Mohamad, A.; Al-Ansary, H. Development of a continuously operating solar-driven adsorption cooling system: Thermodynamic analysis and parametric study. *Appl. Therm. Eng.* **2012**, *48*, 332–341. [[CrossRef](#)]
20. Attalla, M.; Sadek, S.; Ahmed, M.S.; Shafie, I.M.; Hassan, M. Experimental study of solar powered ice maker using adsorption pair of activated carbon and methanol. *Appl. Therm. Eng.* **2018**, *141*, 877–886. [[CrossRef](#)]
21. Ji, X.; Song, X.; Li, M.; Liu, J.; Wang, Y. Performance investigation of a solar hot water driven adsorption ice-making system. *Energy Convers. Manag.* **2015**, *106*, 759–765. [[CrossRef](#)]
22. Rezk, A.R.; Al-Dadah, R.K. Physical and operating conditions effects on silica gel/water adsorption chiller performance. *Appl. Energy* **2012**, *89*, 142–149. [[CrossRef](#)]
23. Elsheniti, M.B.; Hassab, M.A.; Attia, A.-E. Examination of effects of operating and geometric parameters on the performance of a two-bed adsorption chiller. *Appl. Therm. Eng.* **2010**, *146*, 674–687. [[CrossRef](#)]
24. Shaaban, M.; Elsheniti, M.B.; Rezk, A.; Elhelw, M.; Elsamni, O.A. Performance investigation of adsorption cooling and desalination systems employing thermally enhanced copper foamed bed coated with SAPO-34 and CPO-27(Ni). *Appl. Therm. Eng.* **2022**, *205*, 118056. [[CrossRef](#)]
25. Ghazy, M.; Askalany, A.; Kamel, A.; Khalil, K.M.; Mohammed, R.H.; Saha, B.B. Performance enhancement of adsorption cooling cycle by pyrolysis of Maxsorb III activated carbon with ammonium carbonate. *Int. J. Refrig.* **2021**, *126*, 210–221. [[CrossRef](#)]
26. Shabir, F.; Sultan, M.; Miyazaki, T.; Saha, B.B.; Askalany, A.; Ali, D.I.; Zhou, Y.; Ahmad, R.; Shamshiri, R.R. Recent updates on the adsorption capacities of adsorbent-adsorbate pairs for heat transformation applications. *Renew. Sustain. Energy Rev.* **2020**, *119*, 109630. [[CrossRef](#)]
27. Boruta, P.; Bujok, T.; Mika, Ł.; Sztékler, K. Adsorbents, Working Pairs and Coated Beds for Natural Refrigerants in Adsorption Chillers—State of the Art. *Energies* **2021**, *14*, 4707. [[CrossRef](#)]

28. Uddin, K.; El-Sharkawy, I.I.; Miyazaki, T.; Saha, B.; Koyama, S.; Kil, H.-S.; Miyawaki, J.; Yoon, S.-H. Adsorption characteristics of ethanol onto functional activated carbons with controlled oxygen content. *Appl. Therm. Eng.* **2014**, *72*, 211–218. [[CrossRef](#)]
29. Ghazy, M.; Askalany, A.A.; Saha, B.B. Maxsorb III/HFC404a as an adsorption pair for renewable energy driven systems. *Int. J. Refrig.* **2020**, *120*, 12–21. [[CrossRef](#)]
30. Ghazy, M.; Harby, K.; Askalany, A.A.; Saha, B. Adsorption isotherms and kinetics of activated carbon/Difluoroethane adsorption pair: Theory and experiments. *Int. J. Refrig.* **2016**, *70*, 196–205. [[CrossRef](#)]
31. Habib, K.; Saha, B.; Rahman, K.A.; Chakraborty, A.; Koyama, S.; Ng, K.C. Experimental study on adsorption kinetics of activated carbon/R134a and activated carbon/R507A pairs. *Int. J. Refrig.* **2010**, *33*, 706–713. [[CrossRef](#)]
32. Saha, B.; Chakraborty, A.; Koyama, S.; Yoon, S.-H.; Mochida, I.; Ja, M.K.; Yap, C.; Ng, K.C. Isotherms and thermodynamics for the adsorption of n-butane on pitch based activated carbon. *Int. J. Heat Mass Transf.* **2008**, *51*, 1582–1589. [[CrossRef](#)]
33. Rocky, K.A.; Pal, A.; Moniruzzaman, M.; Saha, B.B. Adsorption characteristics and thermodynamic property fields of polymerized ionic liquid and polyvinyl alcohol based composite/CO<sub>2</sub> pairs. *J. Mol. Liq.* **2019**, *294*, 111555. [[CrossRef](#)]
34. Jribi, S.; Miyazaki, T.; Saha, B.B.; Koyama, S.; Maeda, S.; Maruyama, T. Corrected adsorption rate model of activated carbon–ethanol pair by means of CFD simulation. *Int. J. Refrig.* **2016**, *71*, 60–68. [[CrossRef](#)]
35. Elsheniti, M.B.; Elsamni, O.A.; Al-Dadah, R.K.; Mahmoud, S.; Elsayed, E.; Saleh, K. Adsorption Refrigeration Technologies. In *Sustainable Air Conditioning Systems*; IntechOpen: London, UK, 2018; pp. 71–95. [[CrossRef](#)]
36. Zhao, Y.; Wang, L.; Wang, R.; Jin, Z.Q.; Jiang, L.; Fleurance, M. Simulation of heat and mass transfer performance with consolidated composite activated carbon. *Heat Transf. Res.* **2015**, *46*, 109–122. [[CrossRef](#)]
37. Rupa, M.J.; Pal, A.; Saha, B.B. Activated carbon-graphene nanoplatelets based green cooling system: Adsorption kinetics, heat of adsorption, and thermodynamic performance. *Energy* **2020**, *193*, 116774. [[CrossRef](#)]
38. ERG Materials and Aerospace. Aluminium Foam. Available online: <https://ergaerospace.com/materials/duocel-aluminum-foam/> (accessed on 27 May 2020).
39. Sosnowski, M. Evaluation of Heat Transfer Performance of a Multi-Disc Sorption Bed Dedicated for Adsorption Cooling Technology. *Energies* **2019**, *12*, 4660. [[CrossRef](#)]
40. Albaik, I.; Elsheniti, M.B.; Al-Dadah, R.; Mahmoud, S.; Solmaz, I. Numerical and experimental investigation of multiple heat exchanger modules in cooling and desalination adsorption system using metal organic framework. *Energy Convers. Manag.* **2022**, *251*, 114934. [[CrossRef](#)]